Supplementary Material to "Conduit processes at the Haukadalur geyser-hosting hydrothermal field (Iceland) revealed by in-situ temperature and high-speed camera measurements."

Marine Collignon, Laura Pioli, Daniele Trippanera, Aurore Carrier, and Matteo Lupi

We present here additional supporting figures and information in complement to our submitted manuscript. We describe further in details the acquisition and selection of temperature data, the comparison of these data with weather data and finally we provide additional figures and tables for the analyses of temperature oscillations presented in the main manuscript.

1 Temperature data

1.1 Acquisition

We recorded, between 20^{th} and 23^{rd} June 2018, the temperature inside both Strokkur's and Great Geysir's conduits at different depths during several hours at night (Fig. S1).

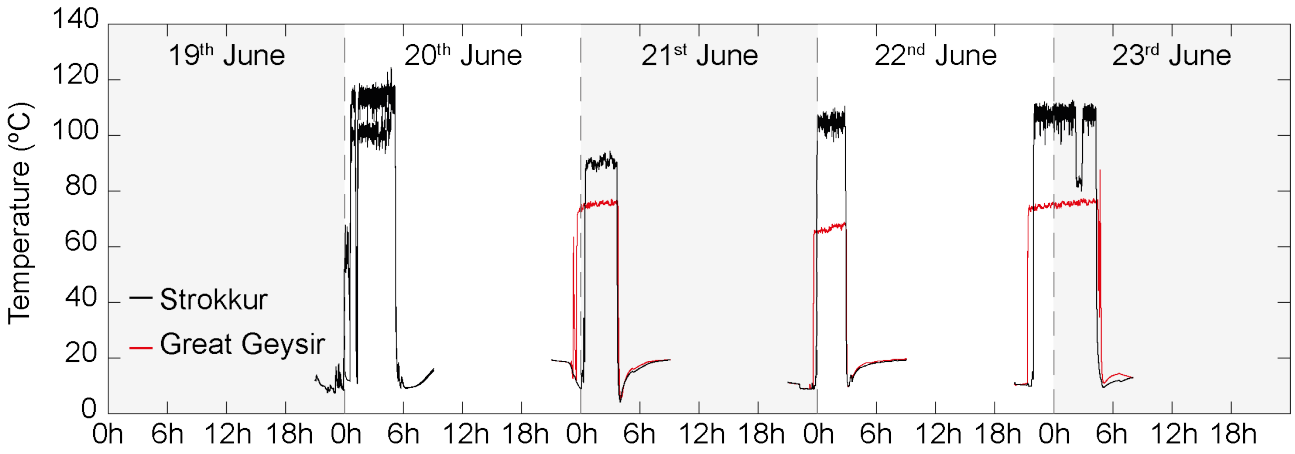

Figure S1. Raw data. Temperature records inside Great Geysir's (red) and Strokkur's (black) conduits are presented with the date and time and without any processing/filtering. Only data acquired with the Hobo U12 sensors are presented here as the Madgetech sensor broke at an early stage of the deployment.

We de- and re-installed the sensors each night because of our working agreement and tourist activity during daytime. Strokkur's eruptions are repeatable and the system is fairly steady (Eibl et al., 2020). Therefore, our recordings at different times can be compared for different eruption types (i.e. single, double or higher order) and conduit depths. On the first night, we lowered inside the conduit two temperature sensors (Hobo U12-015) and one pressure-temperature sensor (Madgetech PRTemp1000), all recording at 1 Hz. Our working agreement allowed us to work from 8 pm to 8 am the next morning. The recording frequency of 1 Hz was chosen based on the internal memory of the sensor to ensure we could record the temperature data during our working time

interval (i.e. 12 hours). This frequency is also sufficiently high to capture heat transfer during an eruption cycle (3.7 ±0.9 min, Eibl et al. (2020)) but not high enough to capture the temperature evolution during the expulsion of a water jet as documented in details by the high-speed camera. After each night, the data were downloaded and the sensors were re-initialised, which reset the memory and the internal clock.

Sensor accuracy ranges from 0.25 to 0.75°C in the range of recorded temperatures (∼80-120°C). The Madgetech sensor was connected to a 2kg fishing weight at the tip of a metallic cable, while the two Hobo sensors were respectively secured at 5 m and 12 m from the bottom of the same cable. The upper part of the cable was regularly marked at 1 m intervals. The system was then inserted inside Strokkur conduit until the cable reached 21 m below the water table. This implies that the two Hobo sensors were recording temperature at a maximum depth of 9 and 16 m inside Strokkur's conduit. Unfortunately, the temperature conditions at 21 m below water exceeded the values that could be withstood by the Madgetech sensor and the instrument broke during deployment after reaching 125°C. Therefore, the temperature recordings could not be associated with precise depths in the conduits. In any case, we consider that the total weight of the equipment (∼2.5 kg, including the fishing weight, cable and sensors) was sufficient to keep the cable vertical and the sensors in place during the eruptions. This hypothesis is supported by the absence of sharp and sudden oscillations in the temperature records just after the eruptions that would have been observed if the sensors were violently pushed up at shallower depths by the vapour slugs before returning to their initial positions. Because of yet possible deviation in the shallowest part of the conduit due to its geometry, it is reasonable to consider that these depth estimates are approximated to 1 m. Similarly, on the three following nights (21^{st}, 22^{nd} and 23^{rd} june), one Hobo U12-015 was deployed inside Strokkur's conduit and the second inside Great Geysir's conduit. The sensors were in this case attached at the bottom of the metallic cables. The sensor inside Strokkur conduit was lowered at about 6, 10 and 11 m below the water table on the 21^{st}, 22^{nd} and 23^{rd} June, respectively. At Great Geysir, the sensor was attached to a weighted metallic cable, which was lowered by 7 m below the water table each night. However, because of the limited weight (< 1kg) and the deployment setup, the cable at Great Geysir was not vertical. According to the slope and size of the geyser pool, we estimated that the thermometer actually reached a depth of 5 m and estimated an uncertainty of 2 m. Therefore temperature at Great Geysir should have been recorded at depths of 3 to 7 m below the water. In this article, the temperature records of Strokkur's conduit on the 20^{th} June at 9 and 16 m and on the following nights are referred to as S20a, S20b, S21, S22 and S23. The temperature records of Great Geyser's conduit between 21^{st} and 23^{rd} June are referred to as G21, G22 and G23. All these temperature data were recorded with the two Hobo U12-015. We did not present the data from the Madgetech sensor as it broke early during one of our first attempts to setup the cable and sensors inside Strokkur's conduit.

1.2 Data selection for analysis

Every night, the Hobo U12-015 sensors recorded the temperature for 12 hours at a frequency of 1 Hz and were re-initialised after downloading the data. The sensors started to record at 9 pm on the first night (S20a

and S20b) and at 8 pm on the three following nights (S21, S22, S23, G21, G22, G23). As shown in Figure S1, the sensors did not only record the temperature inside the geyser conduits but also the air temperature outside and in the equipment box before and after deployment. This explains the sharp jumps from ∼10°C to 70°C and more (Fig. S1). During the first night, we experienced some problems while lowering the cable inside Strokkur's conduit and had to pull out the sensors at the beginning of the deployment. This is visible in the temperature data by rapid drops from water to air temperature. Towards the end of the experiment on the same night, we also experienced some issues while removing the cable with the sensors. The sensors were suddenly and violently sucked down at greater depths, which resulted in an increase in the temperature data. As there are some uncertainties about the depth range for these time intervals, we did not consider the first and last parts of the temperature signal of S20a and S20b. For the three following days, because we aimed at comparing the temperature evolution between Great Geysir and Strokkur, we only considered the time intervals at which both sensors were simultaneously deployed inside the conduits. In the last part of S23, we see a rapid decrease and increase in the temperature that could be linked to a movement of the sensor towards shallower depths and back to its original position after an eruption. We thus did not considered the data of S23, and corresponding G23, after the sharp temperature drop. The selected data represent periods for which we are confident about the estimated depths of the sensors. The selected temperature records do not present any of these sharp and sudden oscillations, suggesting that for the corresponding time intervals the sensors have remained in the range of estimated depths (±).

2 Weather data

Air temperature and pressure, wind speed and precipitation can influence the temperature of pool geysers like Strokkur or Great Geyser. The depth of influence of external weather forcing also depends on the internal dynamics and activity of the geyser. In other words, weather parameters may influence the water temperature at greater depths in quasi-dormant geysers (e.g. Great Geysir) than in active and frequently erupting ones (e.g. Strokkur). Based on the estimated depths of temperature records at Strokkur and Great Geysir, we speculate that changes in weather parameters are unlikely to influence the temperature records at Strokkur but may have an impact at Great Geysir. To verify this assumption and before interpretation of the records with respect to the conduit depths, we analysed the data of two local nearby weather stations between the 18^{th} and 23^{rd} June 2018 (Fig. S2). Unfortunately, there is no weather station in the Haukadalur hydrothermal field. The Hjarðarland and Gullfoss weather stations, respectively located at about 7 km south and 4 km east of Strokkur are the closest stations; the corresponding data could be retrieved from the Urður website (https://urdur.belgingur.is).

Hourly data are available for temperature, relative humidity and wind speed for both Gullfoss and Hjarðarland weather stations (Fig. S3). Data for precipitation are only available at Hjarðarland and are measured as the accumulated rain (in mm), since the last measurement. Rain measurements are taken twice a day at 9 am and 6 pm. The relative humidity can also give a qualitative indication about rain: if it reaches 100%, it is likely raining. Both Gullfoss and Hjarðarland curves show similar evolution but display also small variations,

Figure S2. Location of the weather stations (Gullfoss and Hjarðarland) and the field survey (Strokkur). Source: google map. Coordinates of the weather stations were obtained from https://urdur.belgingur.is. Global coordinates (and location within Iceland) for the field area can be found in the manuscript.

reflecting local conditions. These data represent thus the general trend of the weather in the survey area rather than absolute values representative of the Haukadalur hydrothermal field. This is worth considering as the geothermal field is located at the foot of a small hill, which may locally influence the local weather conditions (e.g. wind speed). The average air temperature during the recording time intervals (vertical grey bars) is similar on the 20^{th} and 23^{rd} June (6 and 7°C, respectively) but slightly lower on the 21^{th} (3°C) and higher on the 22^{nd} (9°C) (Fig. S3a). The general trend of increase and decrease between each night is not always consistent between the air and water temperatures at Strokkur (Table S1). S23 show higher water temperature but lower air temperature than S22. Moreover, changes between different nights in water temperature are much larger than in air temperature. Other weather parameters (relative humidity and wind speed) are also not correlated with the water temperature (Fig. S3b,c and Table S1). During the recording periods, the relative humidity was always around 90-95%, with the exception of the 22^{nd} June, where it reached 100% at Gullfoss. We had some rain in the field that night and the Hjarðarland station shows an increase in accumulated rain before and after the recording period of S22 (Fig. S3d). The wind speed was also low and similar each night during the recording periods, with the exception of the 22^{nd} June, where it increased. The rain and a higher wind speed could also cool down the temperature of geysers in the upper surface. However, S22 presents higher temperature than S21. All these observations suggest that the weather did not influence the observed temperature variations at Strokkur.

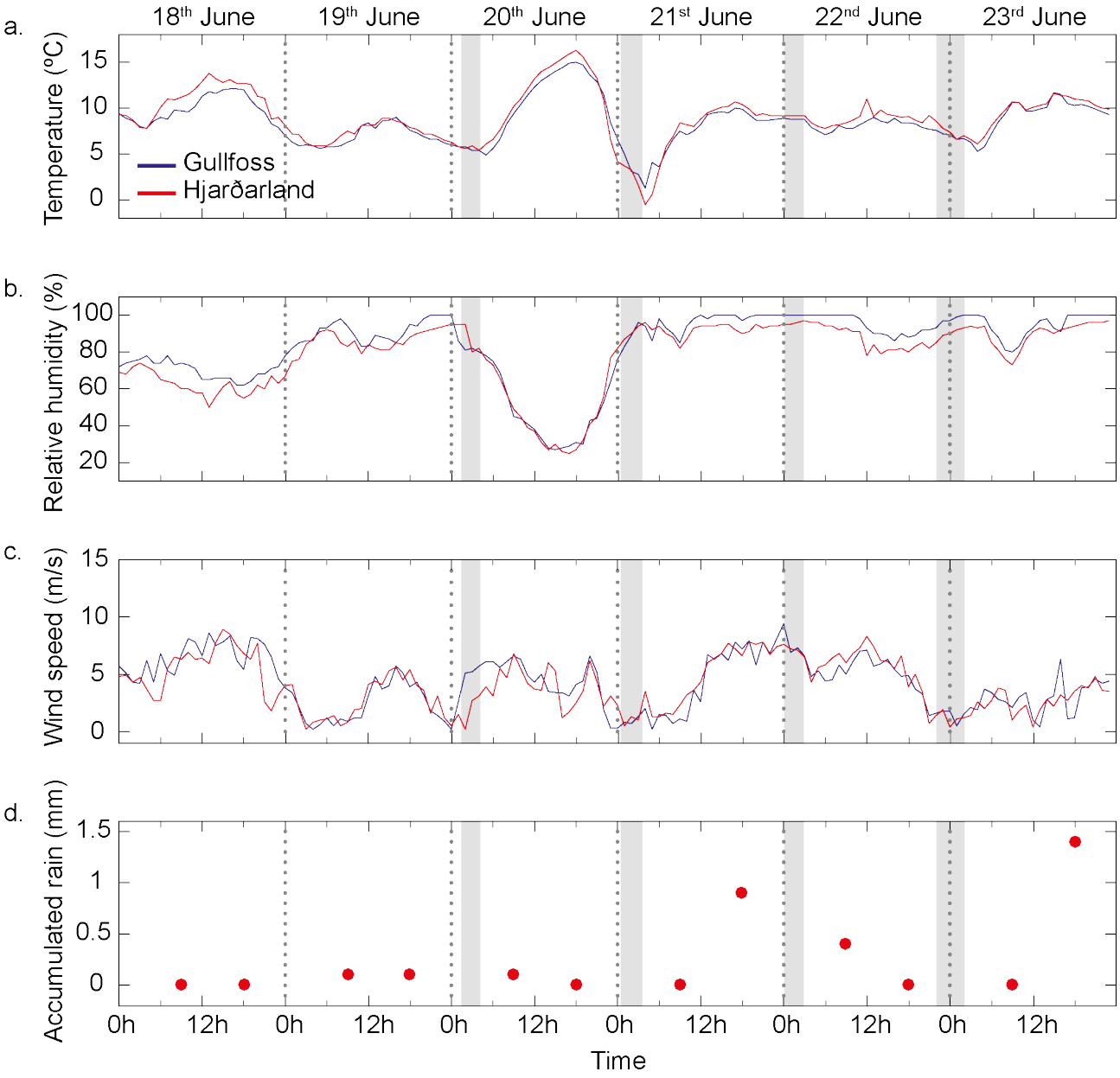

Figure S3. Weather stations. Temperature (a.), relative humidity (b.), average wind speed (c.) and accumulated rain (d.) recorded at Gullfoss (blue) and Hjarðarland (red) weather stations. Data were collected hourly for a., b. and c. Accumulated rain represents the amount of rain since the last measurement at the station. Measurements were taken twice a day, at 9 am and 6pm. Precipitation data are only available at Hjarðarland. Data were obtained from the the Urður website (https://urdur.belgingur.is)

On the contrary, it is possible that changes in weather conditions influenced the water temperature that we recorded at Great Geysir. We observed a much lower temperature for G22 that could be related to the increase in wind speed and precipitation rate during the recording period with respect to the other nights. The temperature drop on the 22^{nd} June is too large to be associated with the 4 m depth range of the recordings in a non-erupting geyser, where the temperature is expected to be constant in the first 10 m below water (Walter et al., 2020). It cannot be associated with the air temperature, which was higher that night.

Recording	G21	G22	G23	S20a	S20b	S21	S22	S23
Depth (m)	5±2	5±2	5±2	9±1	16±1	6±1	10±1	11±1
Water temperature (°C)	75.4	66.7	74.9	100	113	90.2	104.2	106.8
Air temperature (°C)	3	9	7	6	6	3	9	7

Table S1. Average air and water temperature and estimated depth of the sensors at Great Geysir and Strokkur.

3 Oscillations of the temperature signals

Analyses and processing of the temperature records were performed with MATLAB 2016a. Before all analyses, the original temperature records were detrended to remove any potential instrumental drift. The temperature records display quasi-periodic oscillations. We analyse these oscillations and considered that one cycle of oscillation corresponds to the period between two main temperature maxima. For each oscillation cycle, we analyse its cooling phase, between the first maximum and subsequent minimum, and its warming phase between the minimum and the next maximum. Minima and maxima were selected using the findpeaks function in Matlab 2016a. Only the most prominent peaks were selected. We apply as selection criteria a minimum of one minute between each maximum (or minimum) and a prominence of 0.5°C for the peaks at Great Geysir, against 1°C at Strokkur (Figs. S4, S5). We visually inspected the results to ensure the peaks were correctly selected.

For each cooling and warming phases of an oscillation cycle, we characterise the magnitude of the temperature variation (i.e. $|T_{min} - T_{max}|$, in °C) and its associated time (in sec). We then derive the temperature rate (in °C/min) associated with the cooling and warming phases. The statistics (minimum, maximum, mean, median, standard deviation and number of points) of these parameters for the cooling and warming phases of the oscillation cycles are reported in Tables S2 and S3, along with the time interval between maxima.

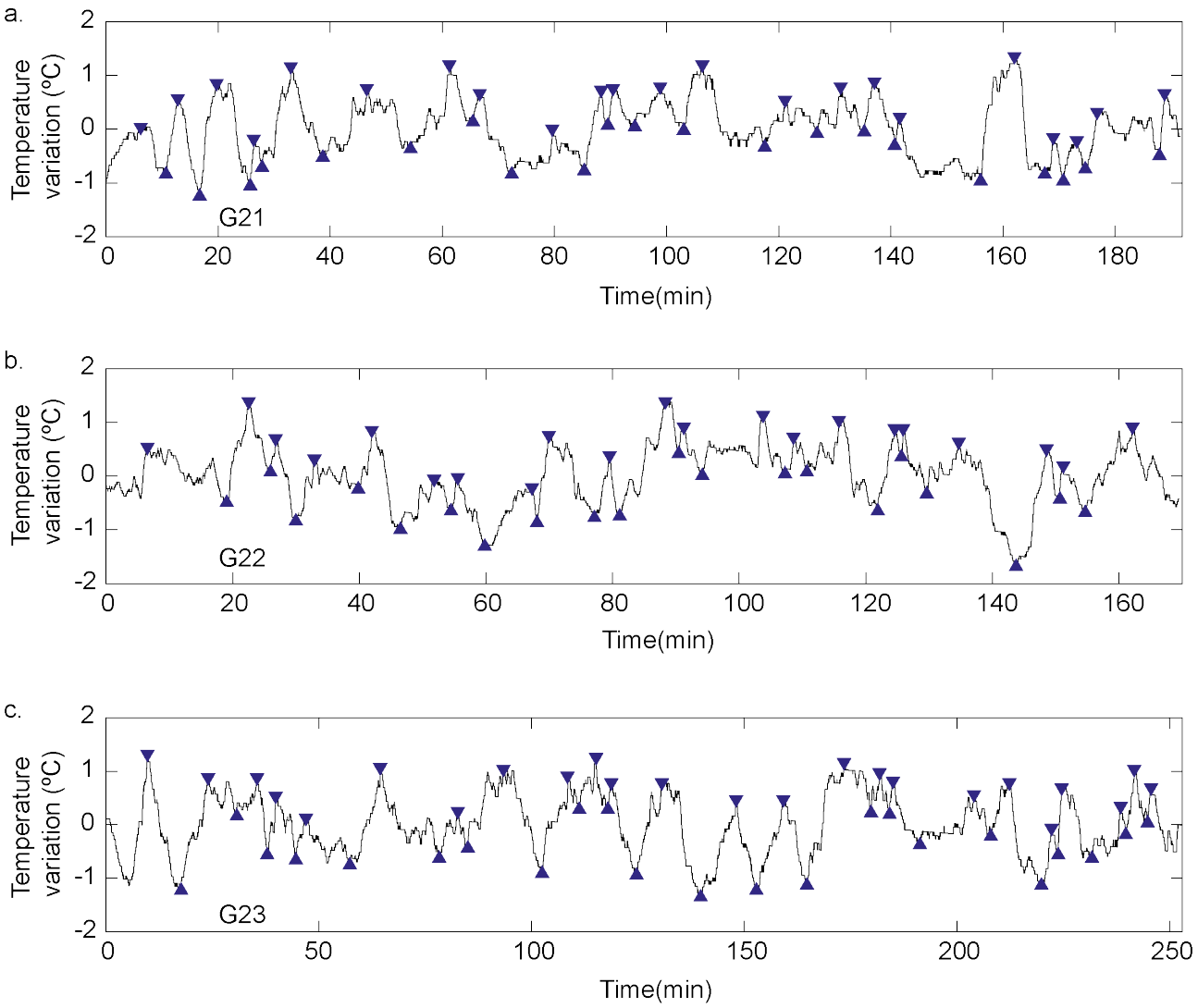

Figure S4. Temperature variations recorded inside Great Geysir's conduit with selected minima and maxima. Oscillation analysis summarised in Table S2. Date, time and depth of the temperature records can be found in the manuscript.

Name	variable	units	mean	std	min	max	median	pts
	ΔT_c	°C	1.11	0.49	0.51	2.18	0.90	21
	Δt_c	sec	324	205	70	873	272	21
	$\Delta T_c/\Delta\ t_c$	°C/min	0.26	0.13	0.07	0.56	0.25	21
G21	ΔT_w	°C	1.14	0.51	0.51	2.30	0.96	21
	Δt_w	sec	198	134	46	467	177	21
	$\Delta T_w/\Delta t_w$	°C/min	0.48	0.29	0.12	1.22	0.49	21
	T_b	sec	523	274	131	1224	419	21
	ΔT_c	°C	1.14	0.47	0.54	2.31	1.07	20
	Δt_c	sec	250	175	53	747	200	20
	$\Delta T_c/\Delta t_c$	°C/min	0.36	0.17	0.08	0.75	0.32	20
G22	ΔT_w	°C	1.16	0.52	0.51	2.18	1.11	20
	Δt_w	sec	217	163	22	576	167	20
	$\Delta T_w/\Delta t_w$	°C/min	0.52	0.35	0.12	1.42	0.48	20
	T_b	sec	467	249	83	964	525	20
	ΔT_c	°C	1.26	0.56	0.52	2.53	1.19	23
	Δt_c	sec	336	190	87	836	339	23
	$\Delta T_c/\Delta t_c$	°C/min	0.26	0.10	0.08	0.55	0.25	23
G23	ΔT_w	°C	1.23	0.51	0.51	2.29	1.06	23
	Δt_w	sec	280	190	40	758	256	23
	$\Delta T_w/\Delta t_w$	°C/min	0.40	0.28	0.07	1.26	0.29	23
	T_b	sec	616	322	148	1141	637	23

Table S2. Statistics of the oscillation cycles for Great Geysir temperature records. T_b corresponds to the time interval between two maxima; ΔT_c, Δt_c and $\Delta T_c/\Delta t_c$ are respectively the magnitude of the temperature variation, the associated time and temperature rate of the cooling phase of the oscillation cycle. ΔT_w, Δt_w and $\Delta T_w/\Delta t_w$ are the magnitude of the temperature variation, the associated time and temperature rate of the warming phase of the oscillation cycle. Min: minimum, max: maximum, std: standard deviation, pts: number of oscillation cycles.

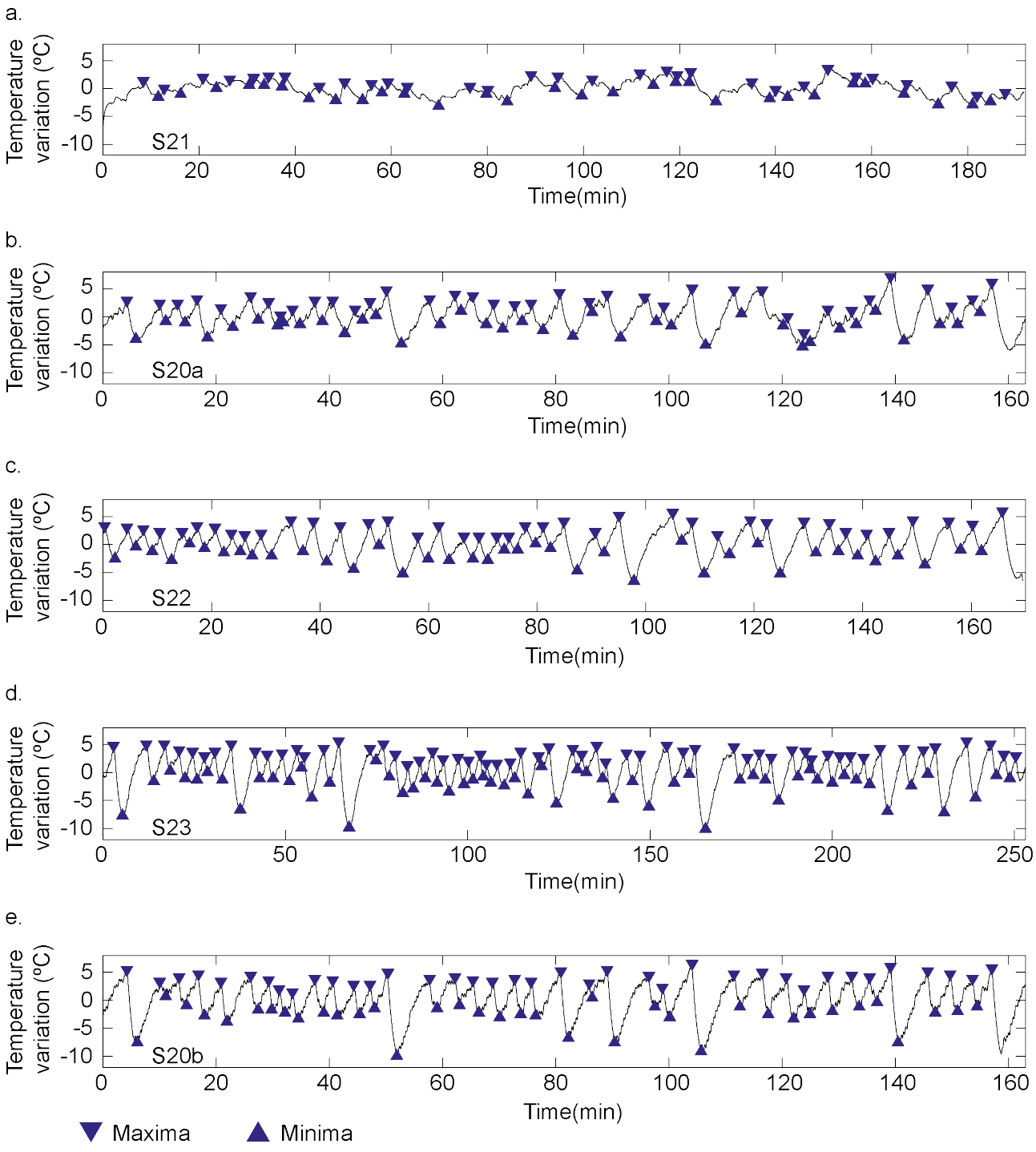

Figure S5. Temperature variations recorded inside Strokkur's conduit with selected minima and maxima. Oscillation analysis summarised in Table S3. Date, time and depth of the temperature records can be found in the manuscript.

Name	variable	units	mean	std	min	max	median	pts
	ΔT_c	°C	2.34	1.02	1.01	5.31	2.20	30
	Δt_c	sec	224	84	114	404	206	30
	$\Delta T_c/\Delta t_c$	°C/min	0.64	0.21	0.25	1.09	0.61	30
S21	ΔT_w	°C	2.27	1.08	1.00	5.00	1.93	30
	Δt_w	sec	135	114	22	439	95	30
	$\Delta T_w/\Delta t_w$	°C/min	1.53	0.92	0.46	3.72	1.37	30
	T_b	sec	359	161	136	794	328	30
	ΔT_c	°C	4.61	2.43	1.40	11.40	4.32	37
	Δt_c	sec	100	40	30	229	91	37
	$\Delta T_c/\Delta t_c$	°C/min	2.78	0.83	1.26	4.53	2.63	37
S20a	ΔT_w	°C	4.69	1.95	1.86	9.99	4.30	37
	Δt_w	sec	148	68	28	310	134	37
	$\Delta T_w/\Delta t_w$	°C/min	2.08	0.74	1.11	5.07	1.95	37
	T_b	sec	248	81	118	452	231	37
	ΔT_c	°C	5.18	2.21	2.19	11.84	4.44	39
	Δt_c	sec	114	24	79	180	108	39
	$\Delta T_c/\Delta t_c$	°C/min	2.64	0.64	1.40	3.99	2.57	39
S22	ΔT_w	°C	5.25	1.99	2.29	12.15	4.91	39
	Δt_w	sec	140	71	48	413	122	39
	$\Delta T_w/\Delta t_w$	°C/min	2.38	0.45	1.62	3.62	2.38	39
	T_b	sec	254	89	130	593	241	39
	ΔT_c	°C	5.87	2.99	1.94	15.46	4.95	58
	Δt_c	sec	102	28	49	188	96	58
	$\Delta T_c/\Delta t_c$	°C/min	3.32	0.82	1.51	5.19	3.29	58
S23	ΔT_w	°C	5.84	3.02	1.92	14.61	4.72	58
	Δt_w	sec	154	88	28	458	127	58
	$\Delta T_w/\Delta t_w$	°C/min	2.42	0.60	1.37	4.46	2.33	58
	T_b	sec	256	112	109	646	215	58
	ΔT_c	°C	6.95	3.26	2.64	15.62	6.07	37
	Δt_c	sec	69	19	38	110	67	37
	$\Delta T_c/\Delta t_c$	°C/min	6.03	1.94	3.18	10.23	5.72	37
S20b	ΔT_w	°C	6.96	2.74	3.32	13.93	6.26	37
	Δt_w	sec	179	74	79	359	163	37
	$\Delta T_w/\Delta t_w$	°C/min	2.40	0.46	1.42	3.52	2.47	37
	T_b	sec	248	83	117	456	232	37

Table S3. Statistics of the oscillation cycles for Strokkur temperature records. T_b corresponds to the time interval between two maxima; ΔT_c, Δt_c and $\Delta T_c/\Delta t_c$ are respectively the magnitude of the temperature variation, the associated time and temperature rate of the cooling phase of the oscillation cycle. ΔT_w, Δt_w and $\Delta T_w/\Delta t_w$ are the magnitude of the temperature variation, the associated time and temperature rate of the warming phase of the oscillation cycle. Min: minimum, max: maximum, std: standard deviation, pts: number of oscillation cycles.

4 Eruption dynamics

Figures and tables below are complementary material to the analyses of the eruptive cycles identified in the temperature data and presented in the main manuscript.

4.1 Analysis of observed eruptions: S22 and S23 data sets

During the nights 22^{nd} and 23^{rd} June, we visually monitored the activity of Strokkur, while recording the temperature inside its conduit. We recorded the timing of the eruption cycles for 46 single, 10 double and 3 triple eruptions. As shown in the main manuscript, each last jet of an eruption (regardless the type) occurs within a few seconds of a temperature maximum. We thus consider that the temperature data could be used as a proxy to identify eruptive cycle. The five seconds delay between the temperature peak and the eruption can be considered as negligible with respect to the duration of the eruptive cycle (3.7 ± 0.9 for single eruption according to Eibl et al. (2020)). An eruptive cycle could thus be identified between two temperature maxima. We used the findpeaks function in Matlab and visually inspected the selected minima and maxima. We then manually removed the selected peaks which were outside of the monitoring periods (see main manuscript). We also manually corrected two aborted eruptions that we noticed during our monitoring. The selected eruption cycles were then classify in single, double and triple eruptions based on our observations. We compared the time interval after eruption (TAE) obtained from our automatic selection with the observed one and found a misfit of less than 5% for 85% of the eruptive cycles but it can reach up to 10% for some of the double and triple eruptions (not all). This may happen if the eruption is more than 5 s away from the peak temperature or if a temperature plateau, rather than a clear peak, is observed before the eruption. In this case, the automatic selection takes the first point of the plateau. This is particularly visible for some of the double and triple eruptions.

Considering an eruptive cycle between two maxima, we can clearly identify a cooling and a warming phase between the minima and maxima. As previously, we characterise for each cooling and warming phases of the eruptive cycles the magnitude of the temperature variation (i.e. $|T_{min} - T_{max}|$, in °C) and its associated time (in sec). We then derive the temperature rate (in °C/min) associated with the cooling and warming phases. The statistics (minimum, maximum, mean, median, standard deviation and number of points) of these parameters for the cooling and warming phases of observed single, double and triple eruptions are reported in Table S4, along with the time interval after eruption (TAE).

Eruption order	variable	units	mean	std	min	max	median	pts
	ΔT_c	°C	4.36	1.27	1.94	7.56	4.39	46
	Δt_c	sec	98	48	49	394	92	46
	$\Delta T_c/\Delta\ t_c$	°C/min	2.82	0.75	0.67	4.07	2.75	46
single	ΔT_w	°C	4.52	1.53	1.92	8.89	4.28	46
	Δt_w	sec	124	49	28	257	120	46
	$\Delta T_w/\Delta t_w$	°C/min	2.35	0.65	1.30	4.46	2.24	46
	TAE	sec	222	72	109	508	213	46
	ΔT_c	°C	9.77	1.49	7.72	11.84	9.68	10
	Δt_c	sec	142	18	117	180	141	10
	$\Delta T_c/\Delta t_c$	°C/min	4.16	0.53	3.39	5.19	3.97	10
double	ΔT_w	°C	9.55	2.15	6.77	12.59	9.64	10
	Δt_w	sec	265	81	157	413	260	10
	$\Delta T_w/\Delta t_w$	°C/min	2.21	0.24	1.76	2.59	2.21	10
	TAE	sec	407	94	294	593	397	10
	ΔT_c	°C	13.91	1.89	11.80	15.46	14.47	3
	Δt_c	sec	173	21	149	188	181	3
	$\Delta T_c/\Delta t_c$	°C/min	4.83	0.26	4.62	5.12	4.75	3
triple	ΔT_w	°C	13.13	2.22	10.58	14.61	14.21	3
	Δt_w	sec	347	106	248	458	334	3
	$\Delta T_w/\Delta t_w$	°C/min	2.34	0.37	1.91	2.56	2.56	3
	TAE	sec	519	125	397	646	515	3

Table S4. Statistics of eruptive cycles observed during the 22^{nd} and 23^{rd} June 2018. ΔT_c, Δt_c and $\Delta T_c/\Delta t_c$ are respectively the magnitude of the temperature variation, the associated time and temperature rate of the cooling phase of the eruptive cycle. ΔT_w, Δt_w and $\Delta T_w/\Delta t_w$ are respectively the magnitude of the temperature variation, the associated time and temperature rate of the warming phase of the eruptive cycle. TAE: time after eruption Min: minimum, max: maximum, std: standard deviation, pts: number of eruptive cycles.

4.2 Analysis of assumed eruptions: S20a and S20b data sets

S20a and S20b records show the synchronous evolution of the temperature at different depths inside Strokkur's conduit. We can thus compare how the warming and cooling phases of eruptive cycles evolve with depth. The previous observation allowed us to identify eruptive cycles from the temperature records using an automatic selection (Figure S6). Results were visually inspected and we corrected the eventual missing/added peaks to obtain the same number of eruptive cycles for S20a and S20b. Considering that S20a was recorded at a similar depth than S22 and S23, we used the results of the previous analysis to identify criteria and thus classify between single, double and triple eruptions. No triple eruptions could be identified. Table S5 summarises the analysis of cooling and warming phases of the selected eruptive cycles.

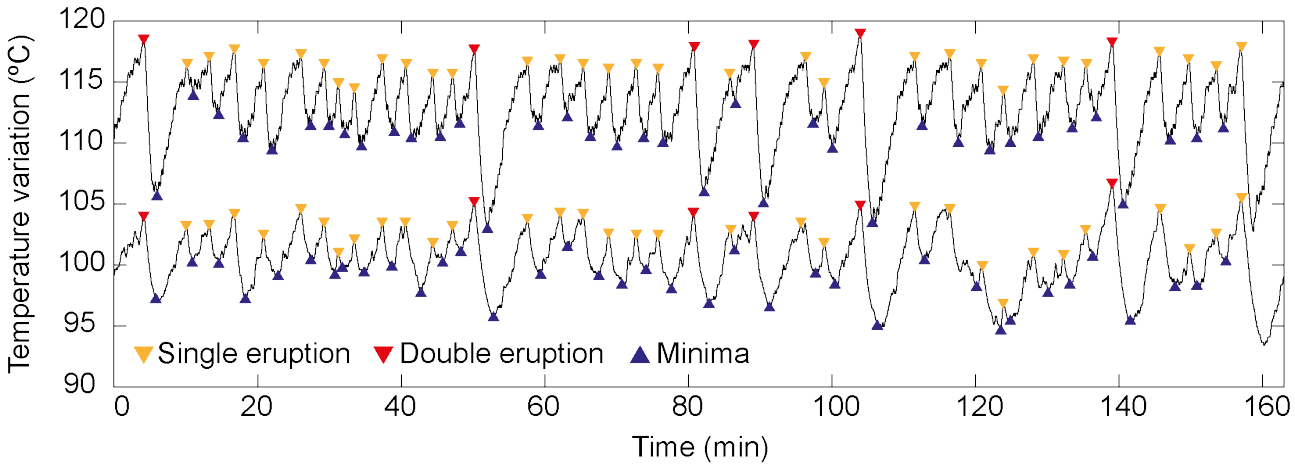

Figure S6. Temperature variations recorded inside Strokkur conduit on the 20^{th} with selected single and double eruptions for the analysis summarised in Table S5. Date, time and depth of the temperature records can be found in the manuscript. The last selected maxima to the right indicates the cycle end of a single eruption. However, based on the subsequent temperature decay this peak probably marks a double eruption.

Record and eruption type	variable	units	mean	std	min	max	median	pts
20a single	ΔT_c	°C	3.79	1.50	1.40	7.08	3.54	31
	Δt_c	sec	93	40	30	229	84	31
	$\Delta T_c/\Delta\ t_c$	°C/min	2.56	0.69	1.26	4.42	2.51	31
	ΔT_w	°C	4.08	1.32	1.86	6.66	4.24	31
	Δt_w	sec	127	48	28	212	127	31
	$\Delta T_w/\Delta t_w$	°C/min	2.12	0.79	1.11	5.07	2.02	31
	TAE	sec	220	48	118	312	216	31
20b single	ΔT_c	°C	5.63	1.22	2.64	7.47	5.65	31
	Δt_c	sec	64	15	38	99	62	31
	$\Delta T_c/\Delta t_c$	°C/min	5.52	1.65	3.18	10.23	5.47	31
	ΔT_w	°C	5.93	1.37	3.32	9.59	5.86	31
	Δt_w	sec	155	48	79	258	151	31
	$\Delta T_w/\Delta t_w$	°C/min	2.39	0.49	1.42	3.52	2.44	31
	TAE	sec	219	48	117	313	210	31
20a double	ΔT_c	°C	8.88	1.73	6.93	11.40	8.62	6
	Δt_c	sec	136	21	99	159	138	6
	$\Delta T_c/\Delta t_c$	°C/min	3.92	0.46	3.41	4.53	3.91	6
	ΔT_w	°C	7.87	1.60	6.15	9.99	7.67	6
	Δt_w	sec	257	46	176	310	261	6
	$\Delta T_w/\Delta t_w$	°C/min	1.86	0.32	1.43	2.28	1.82	6
	TAE	sec	393	55	307	452	398	6
20b double	ΔT_c	°C	13.74	1.29	12.11	15.62	13.38	6
	Δt_c	sec	96	11	85	110	93	6
	$\Delta T_c/\Delta t_c$	°C/min	8.66	0.91	7.11	9.66	8.83	6
	ΔT_w	°C	12.27	1.58	9.92	13.93	12.49	6
	Δt_w	sec	303	59	218	359	322	6
	$\Delta T_w/\Delta t_w$	°C/min	2.47	0.24	2.09	2.73	2.49	6
	TAE	sec	399	60	303	456	416	6

Table S5. Statistics of eruptive cycles observed during the 20^{th} June 2018 at two different depths (S20a: 9±1, S20b: 16±1). ΔT_c, Δt_c and $\Delta T_c/\Delta t_c$ are respectively the magnitude of the temperature variation, the associated time and temperature rate of the cooling phase of the eruptive cycle. ΔT_w, Δt_w and $\Delta T_w/\Delta t_w$ are respectively the magnitude of the temperature variation, the associated time and temperature rate of the warming phase of the eruptive cycle. TAE: time after eruption Min: minimum, max: maximum, std: standard deviation, pts: number of eruptive cycles.

4.3 Analysis of assumed eruptions: S20a, S22 and S23 data sets

Comparison between timing of observed eruption and synchronous temperature records showed that temperature data could be used as a proxy to identify eruptive cycles and characterise their cooling and warming phases (with the exception of S21 that do not show clear oscillations). S20a, S22 and S23 were recorded at a similar depth of ∼10m, considering the 1 m uncertainty. We use these three records to identify and characterise the eruptive cycles on a larger data set (Figs. S7, S8). As previously, the eruptive cycles were automatically selected, visually inspected and corrected if needed based on our observations. The distinction between single, double and triple eruptions was done based on the results of the analysis of observed eruptions (Fig. S7). The analysis of the cooling and warming phases of the selected eruptive cycles is presented in Figure S8 and Table S6.

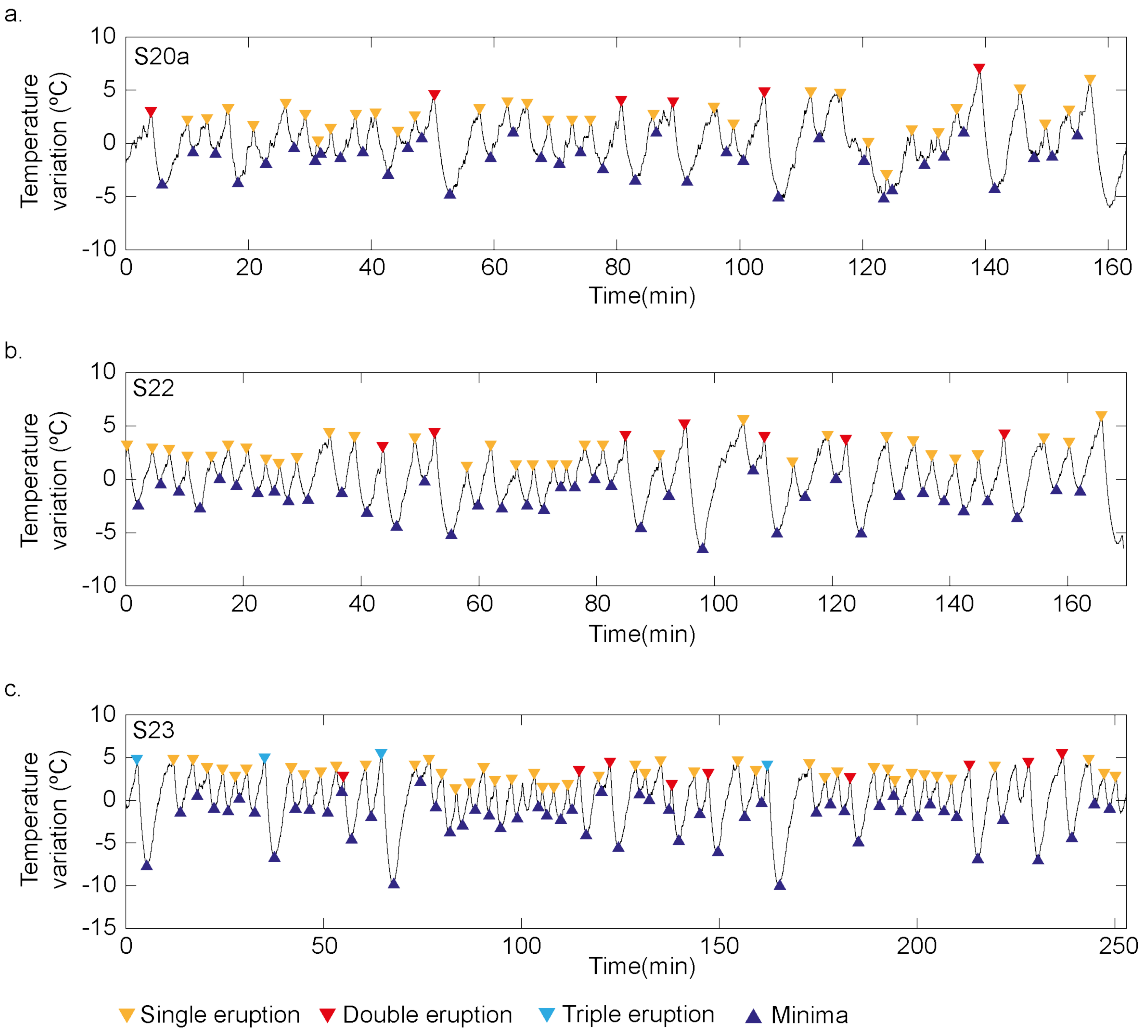

Figure S7. Temperature variations recorded inside Strokkur conduit with selected minima and maxima. Analysis summarised in Table S6. Date, time and depth of the temperature records can be found in the manuscript.

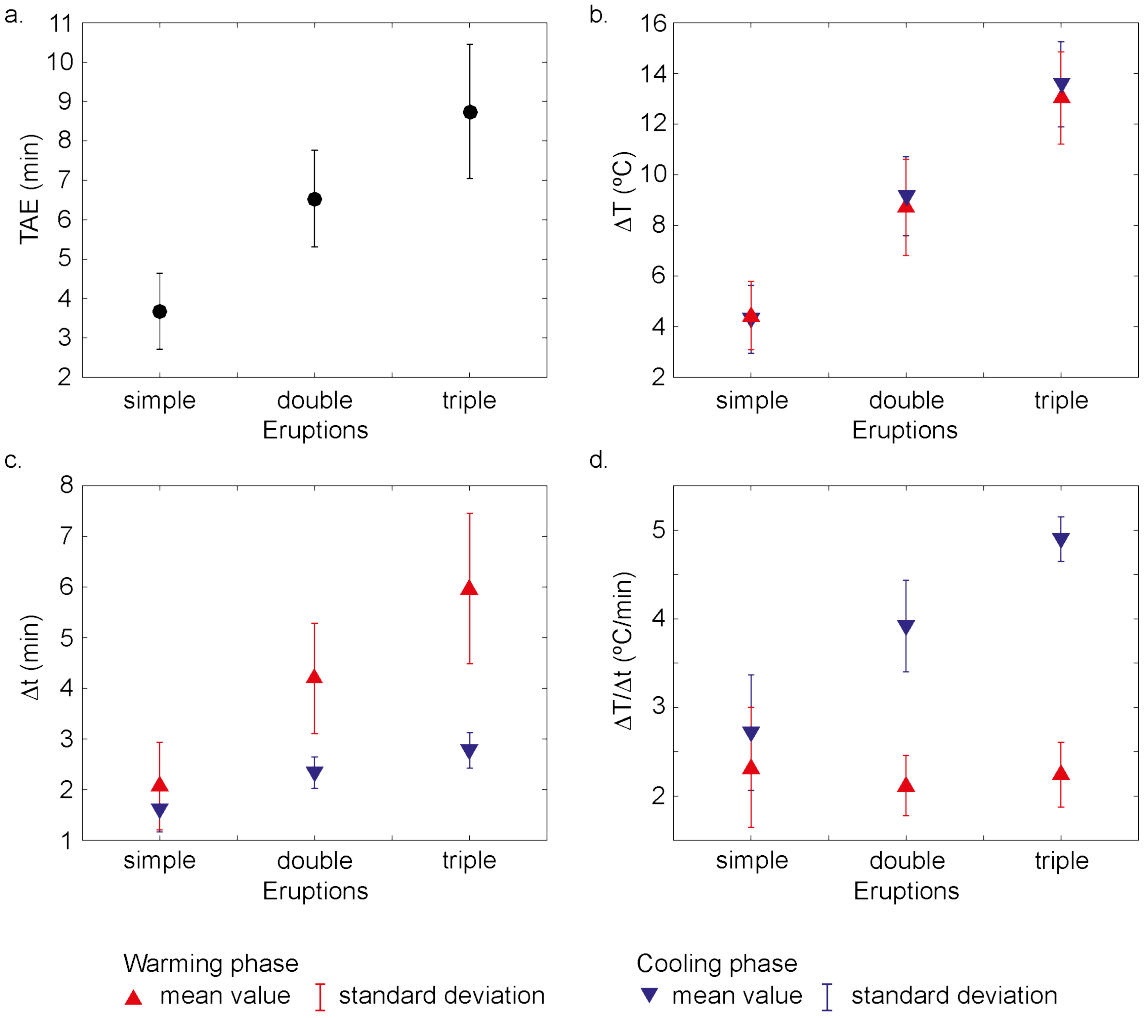

Figure S8. Analysis of eruptive cycles a. TAE as a function of the eruption order. Evolution of the warming and cooling phases of an eruptive cycle as a function of the eruption order. Red: warming phase. Blue: cooling phase. b. temperature variation, c. associated time and d. temperature. Mean value (triangle and circle) and standard deviation (vertical bars) are reported on the graphs. The eruptive cycles were selected from the temperature data (Fig. S7) and further statistics are reported in Table S6

Eruption order	variable	units	mean	std	min	max	median	pts
	ΔT_c	°C	4.29	1.34	1.40	7.56	4.32	107
	Δt_c	sec	96	26	30	229	94	107
	$\Delta T_c/\Delta\ t_c$	°C/min	2.72	0.65	1.26	4.42	2.70	107
single	ΔT_w	°C	4.43	1.35	1.86	8.89	4.29	107
	Δt_w	sec	124	52	28	381	121	107
	$\Delta T_w/\Delta t_w$	°C/min	2.32	0.68	1.10	5.07	2.31	107
	TAE	sec	221	58	109	508	211	107
	ΔT_c	°C	9.14	1.56	6.75	11.84	9.25	21
	Δt_c	sec	140	19	99	180	142	21
	$\Delta T_c/\Delta t_c$	°C/min	3.92	0.52	3.21	5.19	3.95	21
double	ΔT_w	°C	8.71	1.90	6.15	12.59	8.4	21
	Δt_w	sec	252	66	157	413	257	21
	$\Delta T_w/\Delta t_w$	°C/min	2.12	0.34	1.44	2.86	2.15	21
	TAE	sec	392	74	294	593	398	21
	ΔT_c	°C	13.58	1.68	11.80	15.46	13.52	4
	Δt_c	sec	167	21	148	188	165	4
	$\Delta T_c/\Delta t_c$	°C/min	4.90	0.25	4.62	5.12	4.93	4
triple	ΔT_w	°C	13.03	1.82	10.58	14.61	13.46	4
	Δt_w	sec	358	89	248	458	364	4
	$\Delta T_w/\Delta t_w$	°C/min	2.24	0.36	1.91	2.56	2.25	4
	TAE	sec	525	102	397	646	528	4

Table S6. Statistics of the eruptive cycles selected from temperature data (S0a, S22 and S23). ΔT_c, Δt_c and $\Delta T_c/\Delta t_c$ are respectively the magnitude of the temperature variation, the associated time and temperature rate of the cooling phase of the eruptive cycle. ΔT_w, Δt_w and $\Delta T_w/\Delta t_w$ are respectively the magnitude of the temperature variation, the associated time and temperature rate of the warming phase of the eruptive cycle. TAE: time after eruption Min: minimum, max: maximum, std: standard deviation, pts: number of eruptive cycles.

References

Eibl, E., Hainzl, S., Vesely, N., Walter, T., Jousset, P., Hersir, G., & Dahm, T. (2020). Eruption interval monitoring at strokkur geyser, iceland [Journal Article]. *Geophysical Research Letters*, *47*, 1-10.

Walter, T., Jousset, P., Allahbakhsi, M., Witt, T., Gudmundsson, M. T., & Hersir, G. (2020). Underwater and drone based photogrammetry reveals structural control at geysir geothermal field in iceland [Journal Article]. *Journal of Volcanology and Geothermal Research*, *391*, 1-9.